Humic Acid Extracts Leading to the Photochemical Bromination of Phenol in Aqueous Bromide Solutions: Influences of Aromatic Components, Polarity and Photochemical Activity

Hui Liu [1,*], Yingying Pu [1], Xiaojun Qiu [1], Zhi Li [1], Bing Sun [1], Xiaomei Zhu [1] and Kaiying Liu [2]

[1] College of Environmental Science and Engineering, Dalian Maritime University, Dalian 116026, China; py1120181596@dlmu.edu.cn (Y.P.); qiuxiaojun0103@dlmu.edu.cn (X.Q.); lizhi9471@dlmu.edu.cn (Z.L.); sunb88@dlmu.edu.cn (B.S.); zhuxm@dlmu.edu.cn (X.Z.)

[2] School of Science, Dalian Maritime University, Dalian 116026, China; kyliuxw@dlmu.edu.cn

* Correspondence: liuhui@dlmu.edu.cn; Tel.: +86-411-8472-3303

Abstract: Dissolved organic matter (DOM) is considered to play an important role in the abiotic transformation of organobromine compounds in marine environment, for it produces reactive intermediates photochemically and is recognized as a significant source of reactive halogen species in seawater. However, due to the complex composition of DOM, the relationship between the natural properties of DOM and its ability to produce organobromine compounds is less understood. Here, humic acid (HA) was extracted and fractionated based on the polarity and hydrophobicity using silica gel, and the influences of different fractions (F_A, F_B and F_C) on the photochemical bromination of phenol was investigated. The structural properties of HA fractions were characterized by UV-vis absorption, Fourier transform infrared spectroscopy and fluorescence spectroscopy, and the photochemical reactivity of HA fractions was assessed by probing triplet dissolved organic matter ($^3DOM^*$), singlet oxygen ($^1O_2$) and hydroxyl radical ($^{\bullet}OH$). The influences of HA fractions on the photo-bromination of phenol were investigated in aqueous bromide solutions under simulated solar light irradiation. F_A and F_B with more aromatic and polar contents enhanced the photo-bromination of phenol more than the weaker polar and aromatic F_C. This could be attributed to the different composition and chemical properties of the three HAs' fractions and their production ability of $^{\bullet}OH$ and $^3DOM^*$. Separating and investigating the components with different chemical properties in DOM is of great significance for the assessment of their environmental impacts on the geochemical cycle of organic halogen.

Keywords: dissolved organic matter; fractionation; photochemical activity; bromination

1. Introduction

Organohalogen compounds can potentially cause adverse health effects on organisms due to their high cytotoxicity and genotoxicity [1]. The vast majority of organohalogen compounds, especially organobromine compounds, have been identified to originate from natural biotic and abiotic processes in marine environments [2,3]. Apart from approximately 2000 natural organobrimine compounds that are thought to originate from biological processes, it seems that more and more attention has been paid on the abiotic formation pathways of organobromine compounds, especially through photochemical process which has a potential to produce organohalogen compounds within sunlit surface waters [4–6]. For example, phenol, bisphenol A and salicylic acid can be transformed into halogen-containing compounds during sunlight illumination [7–9]. In addition, bromophenols accounted for 93–96% of the total halogenated phenols generating from phenols in coastal seawater upon simulated sunlight irradiation [7], indicating that bromination reactions prevailed over chlorination reactions, though chloride is 760-fold more concentrated than bromide in seawater. However, many uncertainties remain about the yield of

organobromine compounds in natural water, involving the bromination reagent production, the degree of the brominated reaction and its contribution to the organo-bromine pools.

Dissolved organic matter (DOM) is one of the most important natural sunlight absorbing components in aquatic environments and plays an important role in the fate of organic pollutants in natural waters, since the photosensitization of DOM yields a variety of reactive oxygen species (ROS), such as $^\bullet$OH and $^1O_2$ [10–12]. Numerous studies have demonstrated that the effects of DOM on the photodegradation of pollutants are complex, and DOM acts either as a photosensitizer or as an inhibitor depending on its different source and functional groups [13,14]. Increasing attention has been paid on the photochemical process in the presence of DOM and halides. Although halides themselves do not absorb light in the solar region, halides participate in a rich, aqueous-phase chemistry processing initiated by sunlight in the presence of DOM. For example, Parker et al. found that the photodegradation rate of microcystins was faster in saline waters relative to freshwaters in the present of DOM [15]. It was hypothesized that photochemically produced reactive halogen species (RHS), e.g., halogen radicals, might increase the indirect degradation of some pollutants. RHS, including radical RHS (i.e., $X^\bullet$, $X_2^{\bullet-}$ and $XY^{\bullet-}$; where X=Br or I, and Y=Cl) and non-radical RHS (i.e., X_2 and HXO, X=Cl, Br), are seawater-specific photooxidants produced by the oxidation of halides [16]. It was believed that RHS was generated from photochemical processing of DOM, where DOM-induced ROS played an important role [15–17]. The main reaction mechanisms are as follows: first, absorption of sunlight by DOM leads to the generation of ROS, including $^\bullet$OH, H_2O_2 and DOM triplet state ($^3DOM^*$) [18]. Then, bromide is oxidized by the DOM-induced ROS or $^3DOM^*$ to form RHS [19,20]. After that, RHS reacts with other organic matters to form organobromine compounds via addition to unsaturated C−C bonds, recombination with carbon-centered radicals and/or electrophilic substitution [16,21]. However, to our knowledge, little is known on the relationship between RHS production and the natural properties of DOM.

DOM is a mixture of organic compounds with complex molecular compositions and structures, which has large diversity on physicochemical properties, including composition, polarity and aromatic contents, etc. [22]. In order to give a better insight into the structure of DOM, it is often fractionated into a series of less complex fractions. At present, various techniques have been used to separate and characterize DOM. Chromatographic techniques, including high-performance liquid chromatography (HPLC) and size exclusion chromatography, have been employed to separate and identify the functional components within DOM [23,24]. Structural properties such as polarity, hydrophobicity and aromaticity of these obtained DOM fractions are diverse, and thus they present different influences on the environmental behavior of the coexisting organic contaminants [13,23,25]. Moreover, the photo-inductive activities of DOM fractions are different from each other. Remucal et al. reported that DOM formulas with more aromatic and oxygenated components were most efficient at forming $^\bullet$OH but less efficient at producing $^3DOM^*$ and $^1O_2$ [13]. Yu et al. found that the fractions of HA with different polarity that contained varied functional groups appeared to promote or inhibit the photodegradation of 2,4-D [23]. Lee et al. found that DOM with high molecular weight and hydrophobicity significantly inhibited the photolysis of target micropollutants [26]. These results indicate that the DOM separation process based on polarity and hydrophobicity is a good research method to know the relationship between DOM structure and its photochemical properties. However, little information is available for the effects of the fractions with different polarity, hydrophobicity and aromaticity on the photochemical halogenation process.

Several recent investigations have highlighted the photo-initiated halogenation of organic compounds in the presence of DOM [5–9,27], whereas little was done about separating and investigating the components with different chemical properties of DOM and their ability promoting RHS and even halogenation. Herein, HA was fractionated on silica gel into three subcomponents on the basis of their polarity and hydrophobicity, and then HA fractions were characterized and investigated in the process of photochemical bromination of phenol. Silica-gel chromatograph is one of the most popular fractionation

methods for HA, which can separate HA into fractions according to their polarity and affinity toward silica-gel [23,25]. It is expected that more information about the effects of structures and chemical properties of DOM on RHS production and the photo-bromination process can be achieved in this study.

2. Results and Discussion

2.1. Spectroscopic Characterization of HA Fractions

2.1.1. Fourier Transform Infrared Spectroscopy

Figure 1 illustrates the fourier transform infrared (FTIR) spectra of HA fractions (F_A, F_B and F_C). Generally, the spectra of HA fractions show the following bands: OH stretching vibration absorption at 3700–3200 cm^{-1}, C-H stretching vibration absorption of aliphatic series at 2925/2850 cm^{-1}, carbonyl C=O, aromatic C=C, hydrogen-bonded C=O, or COO asymmetrical stretch absorption around 1635/1715 cm^{-1}, the symmetric COO band at 1390 cm^{-1}, and C−O stretching vibration of phenol, alcohols, ethers and/or polysaccharides around 1100 cm^{-1} [28,29]. The relative peak intensities, which reflected the relative amount of each functional group, were different in the spectra of three fractions, indicating their different structural characteristics. Compared with F_C, F_A and F_B showed relatively more intense bands at 1715, 1635, 1390 and 1100 cm^{-1}, indicating that F_A and F_B contained high abundance of aromatic contents, carboxyl and phenolic functional groups.
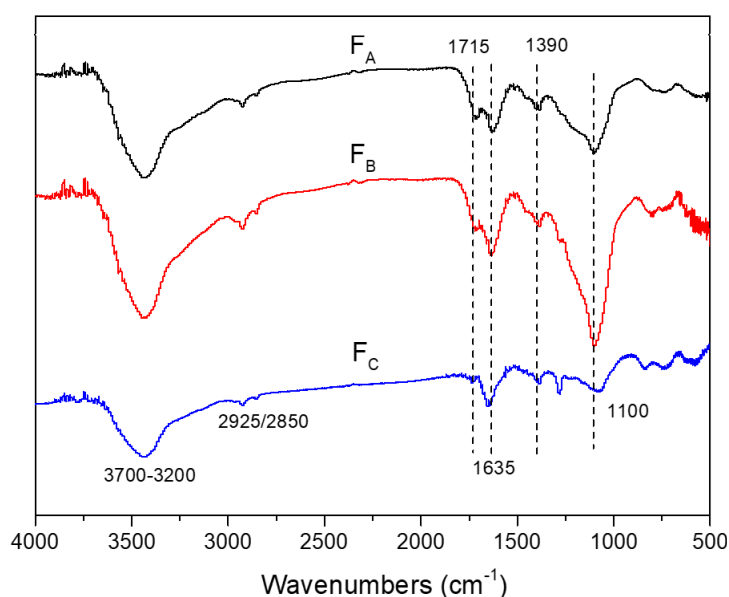

Figure 1. FTIR absorption spectra of three HA fractions.

2.1.2. UV-Vis Spectroscopy

The UV-vis absorption spectra of F_A, F_B and F_C and the lamp emission are presented in Figure 2. The absorption of the three HA fractions varied greatly and their absorption order was $F_A > F_B > F_C$. Korshin et al. reported that a band corresponding to absorption around λ 250 nm designated π-π* transitions in the substituted benzenes or polyphenols [30]. Therefore, the specific-UV absorbance at 254 nm ($SUVA_{254}$) was commonly correlated with the HA aromaticity [13,31]. In addition, the E_{253}/E_{203} ratio was often used to characterize the type of the substituent groups on aromatic rings [32]. A low E_{253}/E_{203} ratio indicates that the substituent groups on aromatic rings are mainly non-polar functional groups such as aliphatic groups, whereas a high E_{253}/E_{203} ratio suggests that the main substituent groups on aromatic rings are polar functional groups such as hydroxyl, carboxyl, carbonyl and ester groups [32,33]. $SUVA_{254}$ and E_{253}/E_{203} of the three fractions are listed in Table 1. The order of $SUVA_{254}$ is $F_A > F_B > F_C$, indicating that F_A contains a relatively high amount of benzenoid and aromatic C=C groups compared with F_B and F_C. Moreover, E_{253}/E_{203} of

F_A was apparently higher than F_B, and F_C showed the lowest E_{253}/E_{203} ratio. These results were well in agreement with the information provided by FTIR that F_A and F_B contained more aromatic components, and F_A contained more polar functional groups on its aromatic rings, such as carboxyl.
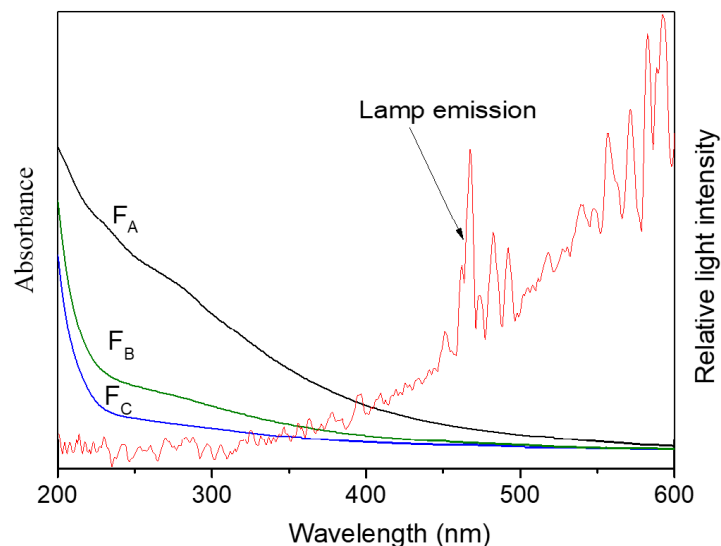

Figure 2. UV-visible absorption spectra of HA fractions and Xenon lamp emission.

Table 1. Spectroscopic properties of HA fractions (F_A, F_B and F_C).

Sample	SUVA [a] (L mg^{-1}m^{-1})	E$_{253}$/E$_{203}$ [b]	EEM [c] Spectra	
			Peak	Property
F_A	4.73	0.65	II, III	Fulvic and humic-like
F_B	1.65	0.32	I, II	Fulvic and protein-like
F_C	0.87	0.22	I	Protein-like

[a] Specific UV absorbance at 254 nm (A254/organic carbon content). [b] Ratio of absorbance at 253 and 203 nm. [c] Three-dimensional excitation-emission matrix fluorescence.

2.1.3. Fluorescence Spectroscopy

Fluorescence spectroscopy has been widely used to characterize DOM in water and soil [32,34,35]. The fluorescence emission spectra of the HA fractions are shown in Figure 3. The $\lambda_{ex}/\lambda_{em}$ of F_A was 360/502 nm with a low intensity, while the $\lambda_{ex}/\lambda_{em}$ of F_B and F_C was lower, at about 360/480 nm. The long wavelength and low intensity measured for the fluorescence peak of F_A indicates the presence of higher amounts of condensed aromatic rings and electron-withdrawing groups (e.g., carboxylic groups) relative to F_B and F_C. On the contrary, the short wavelength and high intensity measured for F_B were associated with the low aromatic content and high electron-donating groups, such as the hydroxyl group [36].

Figure S1 in the Supplementary Materials shows the three-dimensional excitation-emission matrix (EEM) fluorescence spectra of HA fractions. The excitation and emission boundaries were defined into three regions based on previous literature [32,35]. Peaks at shorter excitation wavelengths (<250 nm) and shorter emission wavelengths (<350 nm) are related to simple aromatic proteins such as tyrosine (Region I, Supplementary Figure S1). Peaks at shorter excitation wavelengths (<250 nm) and longer emission wavelengths (>350 nm) are related to fulvic acid-like materials (Region II). Peaks at longer excitation wavelengths (>280 nm) and longer emission wavelengths (>380 nm) are related to humic acid-like organics (Region III). F_A and F_B were mainly composed of fulvic acid and/or humic acid, while F_C was mainly composed of tyrosine-like aromatic proteins. Overall,

the fluorescence peaks varied depending on their polarity and aromaticity (Table 1 and Supplementary Figure S1).
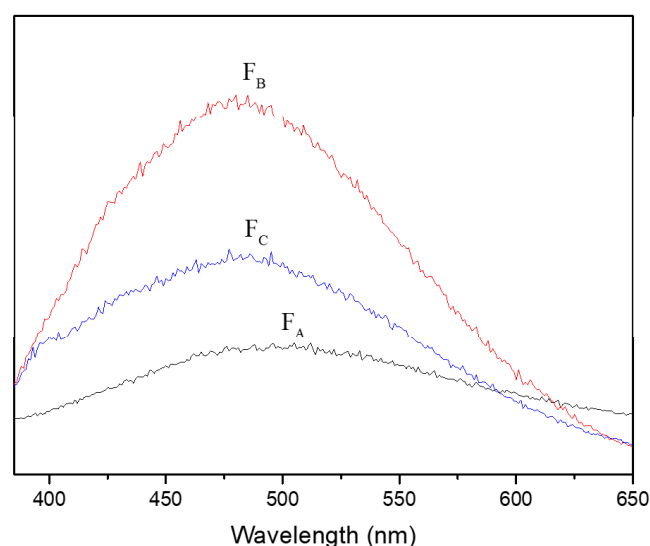

Figure 3. Fluorescence spectra of the HA fractions.

Combining with UV-vis, FTIR and fluorescence data, the spectroscopic properties of HA fractions indicate that F_A consisted mainly of fulvic acid with plenty of aromatic components and polar functional groups on the aromatic rings, F_B was a mixture of fulvic acid with less aromaticity and polarity and F_C comprised mainly tyrosine-like aromatic proteins with low polar groups.

2.2. Photochemical Properties of HA Fractions

2.2.1. Formation of $^3DOM^*$, $^1O_2$ and $^•OH$

The formation rate (R) and the quantum yields (Φ) of $^3DOM^*$, $^1O_2$ and $^•OH$ of three HA fractions solutions and solution rates of light absorbance (R_{abs}) are listed in Table 2. The details can be found in Text S1 and Figure S2 of the Supplementary Materials. For $^3DOM^*$, R_{3DOM} is highest in F_A, and lowest in F_C. However, $\Phi(^3DOM^*)$ is higher in F_B and F_C than F_A. $\Phi(^3DOM^*)$ describes the ratio of R_{3DOM} to light absorption. Positive correlations between absorbance and R_{3DOM} have been observed previously [37]. The charge-transfer model of DOM photochemistry describes long-wavelength absorbance as arising from intramolecular charge transfer interactions between electron-rich donor groups (e.g., hydroxy- or methoxy-aromatic moieties) and electron-poor acceptor groups (e.g., quinones or aldehydes) that are largely derived from the partial oxidation of lignins [10,38]. These compounds should therefore be prevalent in highly aromatic DOM, i.e., F_A. Solution rates of light absorbance significantly influence the quantum yields. Both R_{3DOM} and R_{abs} are higher in F_A than F_B and F_C, and R_{abs} varies by much more than R_{3DOM}, and thus results in lower quantum yields in F_A (Table 2). Therefore, the trend in $\Phi(^3DOM^*)$ across the different HA portion is primarily driven by differences in R_{abs}, rather than R_{3DOM} [38].

Table 2. Quantum Yields (Φ) and formation rates (R) of $^3DOM^*$, $^1O_2$ and $^•OH$, and R_{abs} in solutions containing HA fractions (6.3 mgC L^{-1}). The values were calculated based on Equations (S1)–(S8) of the Supplementary Materials.

	Φ ($^3DOM^*$) $\times 10^3$	$R_{3DOM^*} \times 10^9$ mol L^{-1} s^{-1}	Φ ($^1O_2$) $\times 10^3$	$R_{1O2} \times 10^9$ mol L^{-1} s^{-1}	Φ ($^•OH$) $\times 10^6$	$R_{•OH} \times 10^{12}$ mol L^{-1} s^{-1}	$R_{abs} \times 10^9$ Es L^{-3} s^{-1}
F_A	1.38 ± 0.11	3.31 ± 0.27	2.69 ± 0.19	6.45 ± 0.44	1.49 ± 0.10	3.49 ± 0.26	2.19
F_B	2.47 ± 0.22	3.09 ± 0.27	2.57 ± 0.23	2.98 ± 0.27	2.37 ± 0.28	2.86 ± 0.34	1.23
F_C	2.67 ± 0.29	2.33 ± 0.25	4.31 ± 0.37	3.76 ± 0.33	1.73 ± 0.17	1.51 ± 0.15	0.89

For $^1O_2$, measured $\Phi(^1O_2)$ is highest in F_C. As shown in Table 1, F_C exhibited a typical EEM signature of aromatic protein contents, while the typical components of F_A and F_B were humic acid and fulvic acid. It has been reported that the protein-like components had higher $^1O_2$ quantum yields than that of fulvic acid and humic acid [38,39]. Therefore, F_C was highly efficient at forming $^1O_2$, which was in agreement with previous observations that found that more saturated formulas that are common in microbially derived DOM are strongly correlated with the formation of $^1O_2$ [39].

$^3DOM^*$ is a precursor for $^1O_2$ and the yield for this process is quite high [40,41], thus the order of $\Phi(^1O_2)$ and $\Phi(^3DOM^*)$ was similar to $F_C > F_A$ and F_B. In addition, $\Phi(^1O_2)$ (range = $(2.69 \sim 4.31) \times 10^{-3}$) was almost greater than $\Phi(^3DOM^*)$ (range = $(1.38 \sim 2.67) \times 10^{-3}$) in all fractions. It should be noticed that $^1O_2$ and 2,4,6-trimethylphenol (TMP) likely probe different pools of $^3DOM^*$, which may be attributable to the different $^3DOM^*$ populations capable of reaction with O_2 and TMP, respectively. Almost all triplets that react by energy transfer are theorized to be able to be quenched by O_2, since the singlet energy of O_2 (94 kJ mol^{-1}) is much lower than the reported average triplet energy of DOM (~175 kJ mol^{-1}) [10,40]. In contrast, TMP has a one-electron oxidation potential of 1.22 V, and it reacts by electron transfer with $^3DOM^*$ that has an excited state reduction potential greater than that value [40]. Thus, only triplets with reduction potentials sufficient to oxidize TMP could be detected in $^3DOM^*$ quantification experiments.

For $^\bullet OH$, the $R_{\bullet OH}$ order for HA fractions is $F_A > F_B > F_C$, similar to $^3DOM^*$, whereas, after normalization to the rates of light absorbance, $\Phi(^\bullet OH)$ order was $F_B > F_C > F_A$ (Table 2). In fact, DOM is considered as the main source of $^\bullet OH$ in surface waters [42,43]. The main formation process of $^\bullet OH$ involves the formation of H_2O_2 by irradiated DOM, followed by the generation of $^\bullet OH$ via direct photolysis or photo-Fenton processes. Another $^\bullet OH$ formation is considered via oxidation water by excited DOM. However, conflicting evidence exists about the relationships between the formation of $^3DOM^*$ and $^\bullet OH$. In several studies, DOM samples with the highest $\Phi(^3DOM^*)$ have the highest $\Phi(^\bullet OH)$, implying that $^3DOM^*$ plays the primary role in $^\bullet OH$ formation [11,43,44]. In contrast, other studies concluded that DOM that was highly efficient at producing $^3DOM^*$ was inefficient at forming $^\bullet OH$, suggesting that $^\bullet OH$ was generated through a non-$^3DOM^*$ species precursor [13,45]. Overall, the photoproduction of $^\bullet OH$ is complicated, and the relationship between the composition and properties of DOM and $^\bullet OH$ formation needs further investigation.

2.2.2. Photochemical Bromination of Phenol in the Presence of HA Fractions

The generation of bromophenols in bromide solutions containing different HA fractions under simulated sunlight irradiation are shown in Figure 4. The concentration of bromide, $[Br^-]$, in seawater is at an average concentration of 0.8 mmol L^{-1}, while it is enriched in the sea-spray aerosols due to the evaporation of water and can reach dozens of mmol L^{-1} [46]. Considering the wide $[Br^-]$ range in seawater and aerosol, the bromination of phenol was investigated in the presence of 8 mmol L^{-1} Br$^-$ in this study. The initial phenol concentration is 2 mg L^{-1}, and the concentration of HA fractions is 6.3 mgC L^{-1}. Phenol was irradiated in the reaction solutions and formed two brominated derivatives, 2-bromophenol and 4-bromophenol. The fractions with high aromatic contents and polarity, F_A and F_B, enhanced phenol bromination obviously, and the promotion effects of each fraction on the photo-bromination of phenol varied in the order of $F_A > F_B > F_C$.

As it has been reported previously, phenolic compounds and natural organic substances could be brominated in the sunlit saline solutions or seawaters, where reactive bromine species (RBS) play an important role [5,9,16,19]. RBS includes bromide radicals (Br$^\bullet$/Br$_2$$^{\bullet-}$) and non-radical RBS (HOBr and Br$_2$). The bromine radicals could be generated through oxidation of bromides by $^\bullet OH$ (Equations (1)–(3)) [17,19], or by $^3DOM^*$, such as excited triplet state $^3HA^*$ (Equation (4)) [16], whereas the non-radical RBS could be generated via the recombination of radical intermediates (Equations (5)–(8)). Therefore, the

influence of HA fractions on the bromination of phenol should be focused on the capacity of HA fractions to produce bromine radicals.
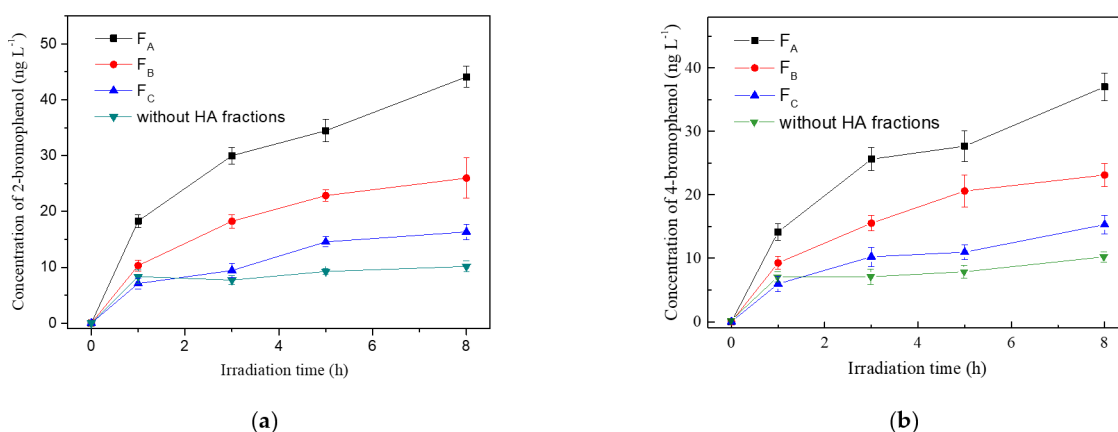
$$\bullet OH + Br^- \rightarrow HBrO^{\bullet -} \tag{1}$$

$$HBrO^{\bullet -} + H^+ \rightarrow Br^\bullet + H_2O \tag{2}$$

$$Br^\bullet + Br^- \rightarrow Br_2{}^{\bullet -} \tag{3}$$

$$^3HA^* + Br^- \rightarrow HA^{\bullet -} + Br^\bullet \tag{4}$$

$$Br^\bullet + Br^\bullet \rightarrow Br_2 \tag{5}$$

$$Br_2{}^{\bullet -} + Br_2{}^{\bullet -} \rightarrow Br_2 + 2\,Br^- \tag{6}$$

$$Br^\bullet + {}^\bullet OH \rightarrow HBrO \tag{7}$$

$$Br_2{}^{\bullet -} + {}^\bullet OH \rightarrow HBrO + Br^- \tag{8}$$

Figure 4. Effects of different HA fractions on the photochemical generation of 2-bromophenol (**a**) and 4-bromophenol (**b**). [phenol]$_0$ = 2 mg L^{-1}, [Br$^-$] = 8 mmol L^{-1} and [HA] = 6.3 mgC L^{-1}.

One important thing we wanted to explore was the relationship between the physico-chemical properties of HA fractions and the photo-bromination reactions. Figure 5 shows that the formation rate of bromophenols was in the order $F_A > F_B > F_C$, which was consistent with the sum of the formation rates (R) of $^3DOM^*$ and $^\bullet OH$ for the three HA fractions. There is no evidence for the generation of RBS from $^1O_2$ yet, and also there was no correlation between formation rate of bromophenols and $^1O_2$. These results indicated that the higher polar and aromatic fraction (F_A) with composition of fulvic acid was prone to produce bromophenols, most probably due to $^3DOM^*$ and $^\bullet OH$ generated by F_A.

Oxidation of bromide by $^\bullet OH$ (E = 2.8 V$_{NHE}$), forming Br radical (E = 1.7–2.0 V$_{NHE}$), is non-selective and has long been recognized as a source of halogen radicals in seawater [16,20]. The production of $^\bullet OH$ from DOM could occur via photo-generated H$_2$O$_2$ from DOM, or oxidation of water and/or OH$^-$ by photochemically excited DOM. However, the relationship between composition of DOM and $^\bullet OH$ formation has not been fully understood yet. Remucal et al. found that DOM formulas with more aromatic components are most efficient at forming $^\bullet OH$ [13]. This finding could support our results that F_A accelerated bromination obviously, since F_A contains higher aromatic contents (Figure 1) and can form $^\bullet OH$ at a higher rate (Table 2), and consequently can generate more RBS. Meanwhile, the formation rate of bromophenols became slow during irradiation, which may be related to the structural change of HA fractions. Various studies have shown that aromatic components of DOM are susceptible to photooxidation and destroyed during irradiation [10,47,48]. The loss of aromatic components might decrease the generation of RBS, and thus slow the bromination rate.
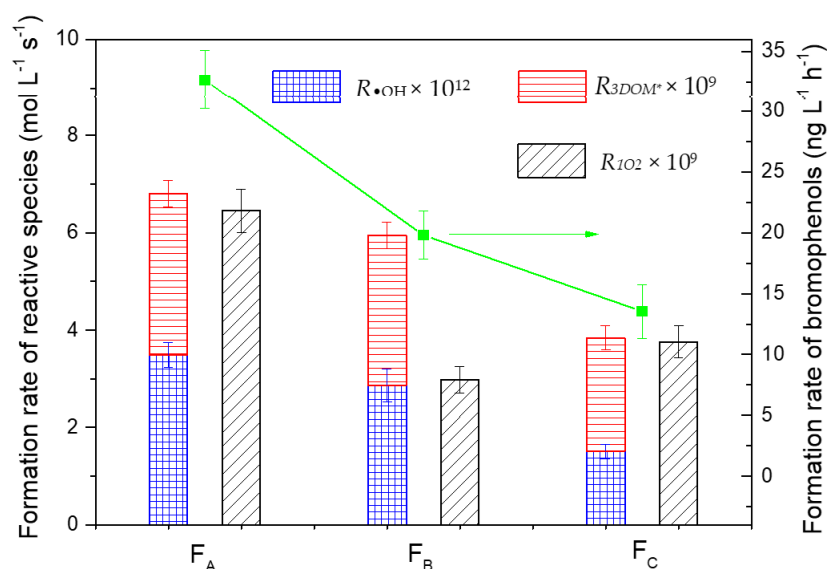
Figure 5. Relationship between the formation rate of reactive species and the total formation rate of bromophenols (2-bromophenol + 4 bromophenol) among three HA fractions. Reaction conditions: $[Br^-]$ = 8 mmol L^{-1}, formation rates of bromophenols are the values calculated at t = 1 h, and the error bars represent one standard deviation.

Another pathway for RBS formation is direct oxidation of bromides by $^3DOM^*$. Parker et al. demonstrated that RBS formation via $^3DOM^*$ oxidation of halides may be a significant RBS generation pathway in coastal seawater [15,17]. As we know, properties of $^3DOM^*$ are clearly different for various structural components [49], and whether $^3DOM^*$ can oxidize bromide ions to radicals depends on its standard reduction potential. Generally, the estimated $^3DOM^*$ reduction potentials ($E(^3DOM^*/DOM^{\bullet-})$ = 1.3−1.9 V_{NHE}) [40] fall within the range of reduction potentials to oxidize halides ($E(Br_2^{\bullet-}/Br^-)$ = 1.7 V_{NHE}) [16]. Moreover, DOM exists as super-molecular aggregates and colloids, where the reduction potential of bromide radical should be lower than in aqueous solutions. The reason is that the estimated reduction potential of bromide radical is about 0.4–0.5 V_{NHE} lower in polar organic solvents, and the electric field in the vicinity of the chromophoric site of DOM may be somewhere in between water and polar organic solvents [40]. Therefore, the oxidation of bromide in the DOM microenvironment should be easier than in water phase.

The aromaticity and polarity of DOM fractions could influence the property of DOM microenvironment. Although the relationship between DOM composition and the oxidizing ability of $^3DOM^*$ is not known yet, it has been reported that some DOM proxies, such as anthraquinone-2-sulphonate, possess a powerful triplet oxidant to be 2.28 V_{NHE} [50]. Thus, it can be supposed that aromatic fractions (F_A and F_B) may have a relatively stronger oxidizing ability of $^3DOM^*$ due to the possible existence of aromatic ketones structures. In addition, the π-π complexes of DOM and phenolic compounds were supposed to impact their photochemical reaction [26]. It has been demonstrated that π-π electron donor-acceptor interactions played an important role between π-donor aromatic compounds and π-acceptor DOM, since DOM contains lots of potentially strong π-acceptor groups, such as quinones and aromatic rings substituted with electro-withdrawing groups such as carbonyl and carboxyl [51]. FTIR spectra demonstrated that F_A possessed more aromatic C=C contents, and UV-vis absorbance (E_{253}/E_{203}) demonstrated that F_A contained more polar groups, such as carboxyl, on aromatic rings. Therefore, the higher aromatic and stronger polar F_A was a stronger π-acceptor than F_B and F_C. It is supposed that F_A and phenol formed stronger complexes than F_B and F_C, which provided a better microenvironment for phenol reaction with reactive species (including both ROS and RBS) to generate bromophenols.

3. Materials and Methods

3.1. Standards and Reagents

Phenol, 2-bromophenol, 4-bromophenol, furfuryl alcohol (FFA), terephthalate (TPA), 2,4,6-trimethylphenol (TMP), *p*-nitroanisole (PNA) and pyridine were purchased from Sigma-Aldrich, and 2-hydroxy-5-chlorobiphenyl was purchased from AccuStandard. All chemicals were with the purity > 98% and used as received. HA was purchased from MP Biomedical, Inc (Eschwege, Germany). Deionized water (18 MΩ cm) was obtained from a Milli-Q system and used in all experiments.

3.2. Fractionation Procedure of HA

The fractionation procedure of HA was described briefly as follows: stock solution of HA was loaded onto a silica gel (60–80 mesh) chromatogram column (Ø30 × 300 mm). A mixture of ethanol and water was selected as the mobile phase and the flow rate was about 1.0 mL min^{-1}. Column effluents were collected as 150 mL aliquots using different volume proportions of ethanol and water in the sequence of the ratio of ethanol:water at 3:7, 4:6 and 5:5, and then three HA fractions, F_A, F_B and F_C, were obtained. Then, the pH of HA solution was adjusted to 1.0 by 6 mol L^{-1} HCl for precipitation, and the precipitates were filtrated and dried at 60 °C for 6 h. The obtained solids were finally dissolved in alkaline solutions (pH 8.5) for total organic carbon (TOC) measurement and used for further experiments.

3.3. Characterization of HA Fractions

The functional groups of HA fractions were analyzed by Fourier transform infrared spectroscopy (FTIR, Nicolet iS 5, Thermo Fisher Scientific, Madison, USA) in the wave number range of 4000 to 400 cm^{-1}. The light absorption properties of HA fractions were characterized using UV-vis spectrophotometry (Hitachi UH5300, Ibaraki, Japan). Fluorescence spectra of the HA fractions were obtained using a Hitachi F-4500 fluorescence spectrophotometer (Japan). The emission spectrum between 380 and 650 nm with excitation at 360 nm was recorded, and excitation-emission matrix (EEM) spectra were obtained by continuous scanning of the emission (Em) wavelength from 220 to 600 nm by increasing the excitation (Ex) wavelength from 200 to 450 nm. TOC was measured using a TOC analyzer (LiquiTOCII, Elementar Analysensysteme GmbH, Langenselbold, Germany).

3.4. Photochemical Experiments

The photochemical experiments were conducted in cylindrical quartz tubes, and the simulated sunlight source (Phchem III, Beijing Newbit Technology Co., Ltd., Beijing, China) contains a 500 W xenon arc lamp and filters to cut off the light with a wavelength below 290 nm. The lamp emission spectrum (shown in Figure 2) was similar to the wave band 290–450 nm of sunlight that plays a main role in photochemical reaction. Photo-productions of ^{3}DOM*, ^{1}O$_2$ and •OH irradiated with a Xenon lamp were quantified using TMP, FFA and TPA as chemical probe molecules, respectively. Experiments were performed in triplicate alongside a *p*-nitroanisole/pyridine actinometer, which was used to quantify light intensity [52]. Experimental details and the determination of photo-formation rates of ^{3}DOM*, ^{1}O$_2$ and •OH are provided in Text S1 of the Supplementary Materials.

3.5. Chemical Analysis

The concentrations of bromophenols were analyzed by gas chromatography mass spectrometry (GC-MS, Aglient 7890B/5977C, Agilent Technologies, Santa Clara, CA, USA) after extraction from aqueous solutions using dichloromethane. The concentrations of TMP and FFA were measured using high-performance liquid chromatography (HPLC) and the concentration of HTPA was detected using a fluorescence spectrophotometer. Details are in Text S2 of the Supplementary Materials.

4. Conclusions

HA was fractionated into three fractions based on the polarity and hydrophobicity using silica gel. F_A consisted of mainly fulvic acid with plenty of aromatic contents and polar functional groups on the aromatic rings, F_B was a mixture of fulvic acid with less aromatic contents and polarity and F_C comprised mainly tyrosine-like aromatic proteins with low polar groups. The promotion order of HA fractions on the photobromination of phenol was $F_A > F_B > F_C$, which was consistent with the order of formation rates of $^3DOM^*$ and $^•OH$ for the different HA fractions. The higher aromatic and polar fraction accelerated phenol bromination due to its production of $^•OH$ and $^3DOM^*$ and the chemical property of the DOM microenvironment. The present work is an attempt to gain new insight into the separation, recognition and assessment of DOM environmental impacts on photochemical formation of organobromine compounds in marine environment.

Supplementary Materials: The following are available online. Text S1: Detailed calculation of formation rate (R) and the quantum yields (Φ) of $^3DOM^*$, $^1O_2$ and $^•OH$ and solution rates of light absorbance (R_{abs}) of the three HA fractions, Text S2: Analysis of bromophenol products, TMP, FFA, HTPA and PNA, Figure S1: EEM fluorescence spectrum of F_A, F_B, and F_C., Figure S2: The curve of each probe molecule and PNA over time under simulated sunlight.

Author Contributions: Conceptualization, H.L. and X.Z.; methodology, Y.P. and H.L.; validation, Z.L. and Y.P.; formal analysis, X.Q. and Z.L.; investigation, Z.L. and Y.P.; resources, B.S. and K.L.; writing—original draft preparation, Y.P. and X.Q.; writing—review and editing, H.L. and Y.P.; funding acquisition, H.L. and B.S. All authors have read and agreed to the published version of the manuscript.

Institutional Review Board Statement: Not applicable.

Informed Consent Statement: Not applicable.

Data Availability Statement: The data presented in this study are available in the article and supplementary material.

Conflicts of Interest: The authors declare no conflict of interest.

References

1. Komaki, Y.; Pals, J.; Wagner, E.D.; Mariñas, B.J.; Plewa, M.J. Mammalian cell DNA damage and repair kinetics of monohaloacetic acid drinking water disinfection byproducts. *Environ. Sci. Technol.* **2009**, *43*, 8437–8442. [CrossRef] [PubMed]
2. Gribble, G.W. The diversity of naturally produced organohalogens. *Chemosphere* **2003**, *52*, 289–297. [CrossRef]
3. Wang, L.S.; Zhou, X.F.; Fredimoses, M.; Liao, S.R.; Liu, Y.H. Naturally occurring organoiodines. *RSC Adv.* **2014**, *4*, 57350–57376. [CrossRef]
4. Leri, A.C.; Ravel, B. Abiotic bromination of soil organic matter. *Environ. Sci. Technol.* **2015**, *49*, 13350–13359. [CrossRef] [PubMed]
5. Méndez-Díaz, J.D.; Shimabuku, K.K.; Ma, J.; Enumah, Z.O.; Pignatello, J.J.; Mitch, W.A.; Dodd, M.C. Sunlight-driven photochemical halogenation of dissolved organic matter in seawater: A natural abiotic source of organobromine and organoiodine. *Environ. Sci. Technol.* **2014**, *48*, 7418–7427. [CrossRef]
6. Hao, Z.N.; Yin, Y.G.; Cao, D.; Liu, J.F. Probing and comparing the photobromination and photoiodination of dissolved organic matter by using ultra-high-resolution mass spectrometry. *Environ. Sci. Technol.* **2017**, *51*, 5464–5472. [CrossRef]
7. Calza, P.; Massolino, C.; Pelizzetti, E.; Minero, C. Solar driven production of toxic halogenated and nitroaromatic compounds in natural seawater. *Sci. Total Environ.* **2008**, *398*, 196–202. [CrossRef]
8. Liu, H.; Zhao, H.M.; Quan, X.; Zhang, Y.B.; Chen, S. Formation of chlorinated intermediate from bisphenolA in surface saline water under simulated solar light irradiation. *Environ. Sci. Technol.* **2009**, *43*, 7712–7717. [CrossRef]
9. Tamtam, F.; Chiron, S. New insight into photo-bromination processes in saline surface waters: The case of salicylic acid. *Sci. Total Environ.* **2012**, *435*, 345–350. [CrossRef]
10. Sharpless, C.M.; Blough, N.V. The importance of charge-transfer interactions in determining chromophoric dissolved organic matter (CDOM) optical and photochemical properties. *Environ. Sci. Processes Impacts* **2014**, *16*, 654. [CrossRef]
11. Dong, M.M.; Trenholm, R.; Rosario-Ortiz, F.L. Photochemical formation of hydroxyl radical from effluent organic matter. *Environ. Sci. Technol.* **2012**, *46*, 3788–3794. [CrossRef] [PubMed]
12. Dalrymple, R.M.; Carfagno, A.K.; Sharpless, C.M. Correlations between dissolved organic matter optical properties and quantum yields of singlet oxygen and hydrogen peroxide. *Environ. Sci. Technol.* **2010**, *44*, 5824–5829. [CrossRef] [PubMed]

13. Berg, S.M.; Whiting, Q.T.; Herrli, J.A.; Winkels, R.; Wammer, K.H.; Remucal, C.K. The role of dissolved organic matter composition in determining photochemical reactivity at the molecular level. *Environ. Sci. Technol.* **2019**, *53*, 11725–11734. [CrossRef]

14. Remucal, C.K. The role of indirect photochemical degradation in the environmental fate of pesticides: A review. *Environ. Sci. Processes Impacts* **2014**, *16*, 628–653. [CrossRef] [PubMed]

15. Parker, K.M.; Reichwaldt, E.S.; Ghadouani, A.; Mitch, W.A. Halogen Radicals Promote the Photodegradation of Microcystins in Estuarine Systems. *Environ. Sci. Technol.* **2016**, *50*, 8505–8513. [CrossRef]

16. Zhang, K.; Parker, K.M. Halogen radical oxidants in natural and engineered aquatic systems. *Environ. Sci. Technol.* **2018**, *52*, 9579–9594. [CrossRef]

17. Dong, Y.X.; Peng, W.Y.; Liu, Y.J.; Wang, Z.H. Photochemical origin of reactive radicals and halogenated organic substances in natural waters: A review. *J. Hazard. Mater.* **2021**, *401*, 123884. [CrossRef]

18. Marchisio, A.; Minella, M.; Maurino, V.; Minero, C.; Vione, D. Photogeneration of reactive transient species upon irradiation of natural water samples: Formation quantum yields in different spectral intervals, and implications for the photochemistry of surface waters. *Water Res.* **2015**, *73*, 145–156. [CrossRef]

19. De Laurentiis, E.; Minella, M.; Maurino, V.; Minero, C.; Mailhot, G.; Sarakha, M.; Brigante, M.; Vione, D. Assessing the occurrence of the dibromide radical ($Br_2^{\bullet-}$) in natural waters: Measures of triplet-sensitised formation, reactivity, and modelling. *Sci. Total Environ.* **2012**, *439*, 299–306. [CrossRef]

20. Mopper, K.; Zhou, X.L. Hydroxyl radical photoproduction in the sea and its potential impact on marine processes. *Science* **1990**, *250*, 661–664. [CrossRef]

21. Heeb, M.B.; Criquet, J.; Zimmermann-Steffens, S.G.; von Gunten, U. Oxidative treatment of bromide-containing waters: Formation of bromine and its reactions with inorganic and organic compounds-A critical review. *Water Res.* **2014**, *48*, 15–42. [CrossRef] [PubMed]

22. Sandron, S.; Rojas, A.; Wilson, R.; Davies, N.W.; Haddad, P.R.; Shellie, R.A.; Nesterenko, P.N.; Kelleher, B.P.; Paull, B. Chromatographic methods for the isolation, separation and characterisation of dissolved organic matter. *Environ. Sci. Processes Impacts* **2015**, *17*, 1531–1567. [CrossRef] [PubMed]

23. Yu, C.Y.; Quan, X.; Ou, X.X.; Chen, S. Effects of humic acid fractions with different polarities on photodegradation of 2,4-D in aqueous environments. *Front. Environ. Sci. Engin. China* **2008**, *2*, 291–296. [CrossRef]

24. Yuan, Y.; He, X.S.; Xi, B.D.; Li, D.; Gao, R.T.; Tan, W.B.; Zhang, H.; Yang, C.; Zhao, X.Y. Polarity and molecular weight of compost-derived humic acid affect Fe(III) oxides reduction. *Chemosphere* **2018**, *208*, 77–83. [CrossRef]

25. Wu, W.; Shan, G.Q.; Xiang, Q.; Zhang, Y.Q.; Yi, S.J.; Zhu, L.Y. Effects of humic acids with different polarities on the photocatalytic activity of nano-TiO2 at environment relevant concentration. *Water Res.* **2017**, *122*, 78–85. [CrossRef]

26. Lee, E.; Shon, H.K.; Cho, J. Role of wetland organic matters as photosensitizer for degradation of micropollutants and metabolites. *J. Hazard. Mater.* **2014**, *276*, 1–9. [CrossRef] [PubMed]

27. Hao, Z.N.; Yin, Y.G.; Wang, J.; Cao, D.; Liu, J.F. Formation of organobromine and organoiodine compounds by engineered TiO2 nanoparticle-induced photohalogenation of dissolved organic matter in environmental waters. *Sci. Total Environ.* **2018**, *631–632*, 158–168. [CrossRef]

28. Karpukhina, E.; Mikheev, I.; Perminova, I.; Volkov, D.; Proskurnin, M. Rapid quantification of humic components in concentrated humate fertilizer solutions by FTIR spectroscopy. *J. Soil. Sediment.* **2018**, *19*, 2729–2739. [CrossRef]

29. Liu, Q.J.; Li, X.; Tang, J.P.; Zhou, Y.M.; Lin, Q.T.; Xiao, R.; Zhang, M. Characterization of goethite-fulvic acid composites and their impact on the immobility of Pb/Cd in soil. *Chemosphere* **2019**, *222*, 556–563. [CrossRef]

30. Korshin, G.V.; Li, C.W.; Benjamin, M.M. Monitoring the properties of natural organic matter through UV spectroscopy: A consistent theory. *Water Res.* **1997**, *31*, 1787–1795. [CrossRef]

31. Weishaar, J.; Aiken, G.; Bergamaschi, B.; Fram, M.; Fujii, R.; Mopper, K. Evaluation of specific ultra-violet absorbance as an indicator of the chemical content of dissolved organic carbon. *Environ. Sci. Technol.* **2003**, *37*, 4702–4708. [CrossRef] [PubMed]

32. Xiao, X.; Xi, B.D.; He, X.S.; Zhang, H.; Li, D.; Zhao, X.Y.; Zhang, X.H. Hydrophobicity-dependent electron transfer capacities of dissolved organic matter derived from chicken manure compost. *Chemosphere* **2019**, *222*, 757–765. [CrossRef] [PubMed]

33. Korshin, G.V.; Benjamin, M.M.; Sletten, R.S. Adsorption of natural organic matter (NOM) on iron oxide: Effects on NOM composition and formation of organo-halide compounds during chlorination. *Water Res.* **1997**, *31*, 1643–1650. [CrossRef]

34. He, X.S.; Yang, C.; You, S.H.; Zhang, H.; Xi, B.D.; Yu, M.D.; Liu, S.J. Redox properties of compost-derived organic matter and their association with polarity and molecular weight. *Sci. Total Environ.* **2019**, *665*, 920–928. [CrossRef] [PubMed]

35. Chen, W.; Westerhoff, P.; Leenheer, J.A.; Booksh, K. Fluorescence excitation-emission matrix regional integration to quantify spectra for dissolved organic matter. *Environ. Sci. Technol.* **2003**, *37*, 5701–5710. [CrossRef] [PubMed]

36. Chen, J.; Gu, B.H.; LeBoeuf, E.J.; Pan, H.J.; Dai, S. Spectroscopic characterization of the structural and functional properties of natural organic matter fractions. *Chemosphere* **2002**, *48*, 59–68. [CrossRef]

37. Maizel, A.C.; Remucal, C.K. Molecular composition and photochemical reactivity of size-fractionated dissolved organic matter. *Environ. Sci. Technol.* **2017**, *51*, 2113–2123. [CrossRef]

38. Maizel, A.C.; Li, J.; Remucal, C.K. Relationships between dissolved organic matter composition and photochemistry in lakes of diverse trophic status. *Environ. Sci. Technol.* **2017**, *51*, 9624–9632. [CrossRef]

39. McCabe, A.J.; Arnold, W.A. Reactivity of triplet excited states of dissolved natural organic matter in stormflow from mixed-use watersheds. *Environ. Sci. Technol.* **2017**, *51*, 9718–9728. [CrossRef]

40. McNeill, K.; Canonica, S. Triplet state dissolved organic matter in aquatic photochemistry: Reaction mechanisms, substrate scope, and photophysical properties. *Environ. Sci. Processes Impacts* **2016**, *18*, 1381–1399. [CrossRef]

41. Haag, W.R.; Hoigné, J. Singlet oxygen in surface waters. 3. Photochemical formation and steady-state concentrations in various types of waters. *Environ. Sci. Technol.* **1986**, *20*, 341–348. [CrossRef] [PubMed]

42. Page, S.E.; Arnold, W.A.; McNeill, K. Assessing the contribution of free hydroxyl radical in organic matter-sensitized photo-hydroxylation reactions. *Environ. Sci. Technol.* **2011**, *45*, 1–11. [CrossRef] [PubMed]

43. Vaughan, P.P.; Blough, N.V. Photochemical formation of hydroxyl radical by constituents of natural waters. *Environ. Sci. Technol.* **1998**, *32*, 2947–2953. [CrossRef]

44. Sur, B.; Rolle, M.; Minero, C.; Maurino, V.; Vione, D.; Brigante, M.; Mailhot, G. Formation of hydroxyl radicals by irradiated 1-nitronaphthalene (1NN): Oxidation of hydroxyl ions and water by the 1NN triplet state. *Photochem. Photobiol. Sci.* **2011**, *10*, 1817–1824. [CrossRef] [PubMed]

45. Glover, C.M.; Rosario-Ortiz, F.L. Impact of halides on the photoproduction of reactive intermediates from organic matter. *Environ. Sci. Technol.* **2013**, *47*, 13949–13956. [CrossRef] [PubMed]

46. Edebeli, J.; Ammann, M.; Bartels-Rausch, T. Microphysics of the aqueous bulk counters the water activity driven rate acceleration of bromide oxidation by ozone from 289–245 K. *Environ. Sci. Processes Impact* **2019**, *21*, 63–73. [CrossRef]

47. Spencer, R.G.M.; Stubbins, A.; Hernes, P.J.; Baker, A.; Mopper, K.; Aufdenkampe, A.K.; Dyda, R.Y.; Mwamba, V.L.; Mangangu, A.M.; Wabakanghanzi, J.N.; et al. Photochemical degradation of dissolved organic matter and dissolved lignin phenols from the Congo River. *J. Geophys. Res.* **2009**, *114*, G03010. [CrossRef]

48. Opsahl, S.; Benner, R. Photochemical reactivity of dissolved lignin in river and ocean waters. *Limnol. Oceanogr.* **1998**, *43*, 1297–1304. [CrossRef]

49. Yang, Y.; Pignatello, J.J. Participation of the halogens in photochemical reactions in natural and treated Waters. *Molecules* **2017**, *22*, 1684. [CrossRef]

50. Canonica, S.; Hellrung, B.; Wirz, J. Oxidation of phenols by triplet aromatic ketones in aqueous solution. *J. Phys. Chem. A* **2000**, *104*, 1226–1232. [CrossRef]

51. Zhu, D.Q.; Hyun, S.H.; Pignatello, J.J.; Lee, L.S. Evidence for π-π electron donor-acceptor interactions between p-donor aromatic compounds and p-acceptor sites in soil organic matter through pH effects on sorption. *Environ. Sci. Technol.* **2004**, *38*, 4361–4368. [CrossRef] [PubMed]

52. Wan, D.; Sharma, V.K.; Liu, L.; Zuo, Y.G.; Chen, Y. Mechanistic insight into the effect of metal ions on photogeneration of reactive species from dissolved organic matter. *Environ. Sci. Technol.* **2019**, *53*, 5778–5786. [CrossRef] [PubMed]